J Appl Electrochem (2013) 43:21–29
DOI 10.1007/s10800-012-0493-2

ORIGINAL PAPER

Ionic conductivity studies and dielectric studies of Poly(styrene sulphonic acid)/starch blend polymer electrolyte containing $LiClO_4$

Y. N. Sudhakar · M. Selvakumar

Received: 24 July 2012 / Accepted: 8 October 2012 / Published online: 21 October 2012

Abstract Proton and lithium-ion conducting biodegradable solid polymer electrolytes were prepared using blends of poly(styrene sulphonic acid) (PSSA) and starch for supercapacitor applications. The ionic conductivities have been calculated using the bulk impedance obtained through impedance spectroscopy with varying blend ratio and plasticizer. Glycerol as plasticizer improved the film formation property, while lithium perchlorate ($LiClO_4$) as dopant enhanced the conductivity. The maximum conductivity has been found to be 5.7×10^{-3} Scm^{-1} at room temperature for 80/20 (PSSA/starch) blend ratio. The dielectric studies showed relaxation peaks indicating proton and Li^+ conduction in the plasticized polymer blend matrix and dielectric modulus also exhibited a long tail feature indicating good capacitance. Differential scanning calorimetry thermograms showed two peaks and decreased with varying blend ratio and plasticizer. A carbon–carbon supercapacitor was fabricated using suitable electrolyte, and its electrochemical characteristics using cyclic voltammetry, AC impedance and galvanostatic charge–discharge were studied. Supercapacitor showed a fairly good specific capacitance of 115 Fg^{-1} at 10 mV s^{-1}.

Keywords Biodegradable polymer electrolyte · Plasticizer · Dielectric studies · Supercapacitor

Y. N. Sudhakar · M. Selvakumar (✉)
Department of Chemistry, Manipal Institute of Technology, Manipal, Karnataka, India
e-mail: chemselva78@gmail.com

1 Introduction

Supercapacitors (SCs) are considered as one of the most promising electrochemical energies which stores electrical energy through double-layer charging, faradaic processes, or a combination of both. The amount of energy stored is usually small and can be delivered instantaneously, making supercapacitor devices able to provide pulsed high power rather than high amount of energy, which complement secondary batteries [1]. SCs are widely investigated in many potential applications including memory backups, hybrid power systems for electric vehicles, military, medical applications and digital communications [2]. SCs can be made from a variety of materials, selection of which largely depends on the type of capacitance to be utilised. Carbon in its dispersed and conducting form is the most widely used commercial material for SCs. These materials can be obtained by an activation pre-treatment of existing carbon materials made initially from thermal carbonization of coal, pitch, wood, coconut shells or polymers [1]. To provide flexibility and reduce the risk of leakage from conventional liquid electrolyte containing SCs, solid polymer electrolytes were extensively studied by many researchers [3–5].

Solid polymer electrolytes obtained from natural polymers such as starch, chitosan, pectin, etc., have attracted attention in recent times because of their superior mechanical and electrical properties [6, 7]. Victoria [7] in a mini-review provided an information which presented the viability of using naturally occurring polysaccharides for bio-based electro-active polymers in applications such as batteries, anticorrosion technology, tissue engineering, actuators, electrochromic paper, molecular wires and biosensors. The use of renewable resources to produce blended bio-based products will affect the worldwide

dependence on petroleum-based and synthetic products and feed stocks. Since 1970s, starch has been incorporated into polyethylene to enhance its biodegradability. Biodegradable composites of poly(propylene carbonate) reinforced with unmodified granular corn starch have been studied by several researchers [8, 9]. Gelatinization (or plasticization) of starch is also a good method to enhance the interfacial affinity [10]. A proton-conducting polymer electrolyte based on starch and ammonium nitrate (NH_4NO_3) was reported by Khiar et al. [11], wherein the amount of NH_4NO_3 was found to influence the proton conduction and the highest obtainable room temperature conductivity was 2.83×10^{-5} Scm^{-1}. Arrieta et al. [12] reported on preparation of starch-based biofilm and with varying amount of plasticizers and lithium perchlorate ($LiClO_4$) and exhibited that starch can conduct Li ion. Due to the polyfunctionality of starch, its use in polymer blends seems to be interesting to obtain biodegradable polymer electrolyte. The fact that starch has –OH free groups, which is able to interact by hydrogen bonding with other functionalized polymers, is a starting point to obtain new biodegradable blends.

The use of functionalized polymers represents a good way to obtain interacting polymers which can produce a single-phase material or a compatible blend with enhanced properties. A special class of functionalized polymers with the electrolytic groups attached to the polymeric backbone is polyelectrolyte. Commonly, polyelectrolytes will dissociate into ions in polar solvents, resulting in charged polymer chains and oppositely charged counter ions [13]. In the solid state, only the counter ions are mobile. The combined advantages of the high ionic conductivity of electrolytes and the mechanical properties of polymers render polyelectrolytes an attractive candidate for solid-state supercapacitor. In general, proton-conducting polymers are usually based on polyelectrolytes, which have negatively charged groups attached to the polymer backbone.

Poly(styrene sulphonic acid) (PSSA) is a polyelectrolyte which can be produced by direct sulphonation of commercially available polystyrene [14]. Humidified PSSA has high proton conductivity, and for a short period, it can be used as a polymer electrolyte membrane in fuel cells [15]. Further, Acar et al. [16] prepared poly(2,5-benzimidazole)/PSSA blend membranes which have thermomechanical stability and illustrated sufficient proton conductivities under low humidity conditions. Wee et al. [17] explained PSSA as an effective ion conducting electrolyte medium in supercapacitors with electrodes based on carbon nanotube networks, where ionic conductivity reached up to 4×10^{-4} Scm^{-1} at 80 % relative humidity. These polyelectrolytes tend to be rather rigid and are poor proton conductors unless water is absorbed. So in the present work, starch was our choice to blend with PSSA, and glycerol was selected as proper plasticizer. Glycerol has good compatibility with starch [18] and also improves film forming properties due to the presence of hydroxyl groups [19]. Although PSSA has considerably good conductivity, addition of starch will decrease the conductivity of the system to an extent. Therefore, $LiClO_4$ was added to maintain high conductivity in the system. Doping with $LiClO_4$ reduces local viscosity, thereby, facilitating the mobility of ions such as Li^+ within the medium, which in turn enhances the electrical conductivity [20] along with proton conduction in polymer electrolyte. As a part of our ongoing research programme on biodegradable polymers [21–23], we have previously reported for the first time a polymer electrolyte based on a biodegradable blend polymers, chitosan and poly(ethylene glycol), with different concentrations of $LiClO_4$ and plasticizer [24]. Therefore, in this work, we investigate the use of blend polymer electrolyte containing plasticized $LiClO_4$-doped PSSA/starch film for use in supercapacitor. At the temperature range of 298–343 K, electrical conductivity, dielectric constant and dielectric loss as well as the real and imaginary parts of the electrical modulus were analysed for solid blend polymer electrolytes containing different blend ratios. The surface characterisation was done using scanning electron microscope (SEM). In addition, the effect of the temperature on the plasticized and non-plasticized blend polymer electrolytes was studied using differential scanning calorimetric (DSC) technique. The specific capacitance of fabricated supercapacitor based on a blend polymer electrolyte (PSSA/starch) was characterized and compared using impedance spectroscopy, cyclic voltammetry (CV), and galvanostatic charge–discharge techniques.

2 Experimental

PSSA ($M_n = 88 \times 10^3$) was purchased from Polymer Source Inc. and soluble starch from Merck. Glycerol from Aldrich was used as such without further purification. $LiClO_4$ (Aldrich) was dried at 393 K and kept under vacuum for 48 h before use. 2 % (*w*/*v*) PSSA solution was prepared by dissolving in double distiled water and similarly 2 % (*w*/*v*) starch in double distiled water was prepared separately. These polymer solutions were used as stock solutions. PSSA/starch blend solutions were prepared by mixing the appropriate amount of these stock solutions with plasticizer and salt, respectively, as S1-74 (90/10): 25:1 (wt %); S2-74 (80/20): 25:1 (wt %); S3-74 (70/30): 25:1 (wt %); S4-74 (60/40): 25:1 (wt %); S5-74 (50/50): 25:1 (wt %) and S6-99 (80/20): 0:1 (wt %) for ionic conductivity studies. Along with S6, $LiClO_4$-doped PSSA/starch blend solutions without plasticizer as S7-99 (90/10): 0:1 (wt %); S8-99 (70/30): 0:1 (wt %) for thermal studies. The so-prepared

blend solutions were casted as films on clean petri dishes. Solid blend polymer electrolytes were dried initially at room temperature and then were kept in a vacuum oven at 50 °C for 48 h to complete dryness before subjecting to various studies. SEM analysis was performed using JEOL JSM-6380LA instrument.

DSC measurements of the $LiClO_4$-doped PSSA/starch blend samples were done on a DSC-60 Model instrument from Shimadzu, Japan. Measurements were performed over a temperature range of 30–200 °C at a heating rate of 10 °Cmin^{-1} under the nitrogen atmosphere. T_g values of the blends were evaluated from the first heating curves.

Biodegradation behaviour of the $LiClO_4$-doped PSSA/starch blend films has been studied for samples S6–S8 and S2 using activated sludge degradation method [25–27]. Activated sludge in the form of slurry was collected from waste treatment plant that treats rejected products from BASF industry. The characteristics of sludge and the method can be found elsewhere [28]. To explain briefly, the pre-weighed blend films were kept immersed in activated sludge contained in different jars and were aerated intermittently by air bubbling using a pump, to keep aerobic condition. The films were removed from the sludge solutions after 5, 10 and 15 days, washed well with double distiled water, dried in a hot air oven at 75 °C to perfect dryness and weighed to know the degradation in the intervals of 5, 10 and 15 days. The test was reproducible within ±3 % error.

2.1 Electrochemical studies

Samples were cut into 1 cm^2 area and placed between two square copper electrodes fitted with copper wires. The whole setup was held tightly with a plastic clamp. The bulk ionic conductivities (σ) and dielectric properties of the blends were determined from the electrochemical impedance spectra (EIS) in the frequency range between 1 and 100 MHz using a small amplitude AC signal of 10 mV. Experiments were carried out at temperature range of 298–343 K using proportional-integral-derivative controlled oven from SES instruments Pvt. Ltd. The formulas and relationships between complex impedance, admittance, permittivity and electrical modulus can be found elsewhere [28, 29].

2.2 Fabrication of symmetrical supercapacitor cell

Electrode material for supercapacitor fabrication was prepared using activated carbon (AC) derived from areca fibres having surface area 250 m^{2}g^{-1}. AC was coated on stainless steel electrode using poly(vinylidene fluoride) as binder. The supercapacitor cell was constructed using $LiClO_4$-doped plasticized PSSA/starch blend film sandwiched between two AC-coated electrodes. Electrochemical characterizations were carried out by cyclic voltammetry (CV), EIS and galvanostatic charge–discharge studies. All the electrochemical studies were carried out using a BioLogic SP-150 electrochemical system.

3 Results and discussions

3.1 Ionic conductivity studies

The bulk ionic conductivities (σ) of the blend polymer electrolytes have been determined from the complex impedance using the equation, $\sigma = L/RA$, where L, R and A are the thickness, bulk resistance and area of the solid polymer electrolyte, respectively. The bulk resistance was calculated from the high frequency intercept on the real impedance axis of the Nyquist plot [30] as a function of temperature. The temperature dependence of conductivity for the varying PSSA/starch blend ratios with fixed plasticizer and salt contents has been shown in Fig. 1. The conductivity values are found in the range of 10^{-2}–10^{-5} Scm^{-1} for various samples of PSSA/starch blend polymer electrolytes. The plot shows that as temperature increases, the conductivity increases with non-linear pattern. On addition of plasticizer, the conductivity value increases to $\sim 10^{-2}$ Scm^{-1}. The effectiveness of glycerol in biodegradable blend films from PSSA/starch blend is most likely due to its small size, and it could cluster itself at high concentration decreasing the starch–PSSA chain hydrogen bonding. As a result, dissociation of the dopant salt increases and thereby enhancing Li^+ ion conductivity. As there is an increase in the PSSA concentration (S1–S5) along with an increase in temperature, it seems that the

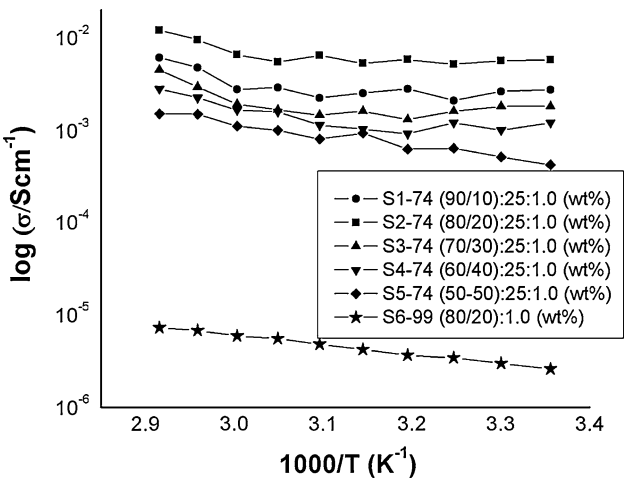

Fig. 1 Variations of conductivity in different compositions of blend (PSSA/starch) polymer electrolyte, salt and plasticizer ($LiClO_4$: glycerol) contents with different temperature

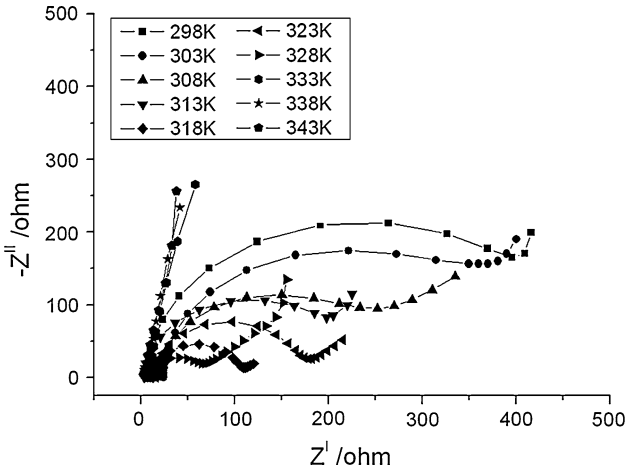

Fig. 2 Nyquist impedance plots of the sample (S2) biodegradable polymer electrolyte at different temperatures

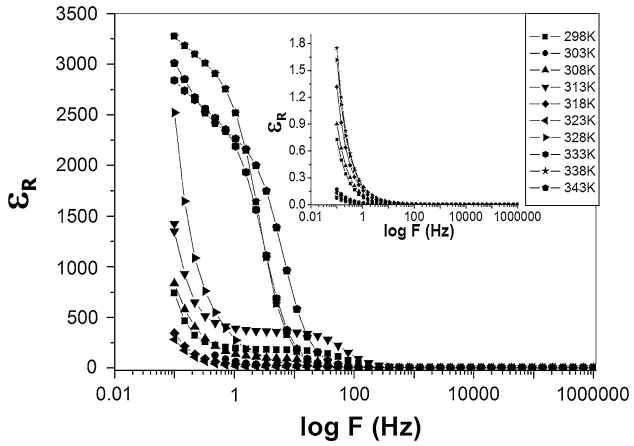

Fig. 3 Plots of dielectric constant versus frequency at different temperatures [*inset* without plasticizer (S6)]

mechanism of ionic conduction behaves as the Vogel–Tammann–Fulcher model, where the ionic transport is promoted by segmental motion which is surrounded by viscous matrix of plasticizer [31]. The highest ionic conductivities were obtained from the sample S2, and the values were 5.7×10^{-3} Scm^{-1} at 298 K and 1.2×10^{-2} Scm^{-1} at 343 K. The ionic conductivity was less in S1 although PSSA content is high, due to the intermolecular bonding between PSSA and starch which decreases the dissociation of doped salt. This shows blending of polymers increases the conductivity better than the individual polymer electrolytes as reported in the literatures [12, 17]. Although 68 wt% of glycerol was taken as plasticizer in the literature [32] for the pectin-based natural gel polymer electrolyte, the ionic conductivity was 4.7×10^{-4} Scm^{-1} at room temperature, which is much less compared to our system. Ionic conductivity value for the sample without plasticizer (S6) was 2.7×10^{-5} Scm^{-1} at 343 K. Figure 2 shows the Nyquist plot for calculation of bulk resistance from the high frequency intercept on the real impedance axis for the sample S2 as a function of temperature. As observed, the resistance of the films decreases as the temperature increases. Increase in temperature leads to further increase in segmental motion of starch molecules within plasticizer phase forming immiscible blends [33].

3.2 Dielectric analysis

Figure 3 shows dielectric constant (ε_R) as a function of frequency with glycerol as plasticizer (S2) at different temperatures and inset Fig. 3 shows without plasticizer (S6). At lower frequency, the ε_R value of the plasticizer sample is much (up to 3,000 times) higher than without plasticizer. This is due to enhanced charge carriers in the space charge accumulation region [34] and thus conductivity increases. The dielectric constant increases sharply towards the low-frequency region which is attributed to the contribution of charge accumulation at the electrode/electrolyte interface, since Li^+ and protons are unable to exchange with the blocking electrodes. The observed space charge regions with respect to the frequency can be explained through ion diffusion where the behaviour is generally known as the non-Debye type. As frequency increases, the ε_R decreases due to the high periodic reversal of the electric field at the interface, which reduces the contribution of charge carriers towards the electrode. Also, the dispersion shifts towards the high-frequency region as the temperature increases. The high-frequency saturation indicates the orientation of dipoles in the direction of the applied electric field decreases in the sample with plasticizer and thereby enhancing the Li^+ and proton mobility [35]. As the temperature increases, the dielectric constant increases due to the enhanced conductivity at higher temperature.

To study the free charges built up at the interface between the materials and the electrodes, the variations of dielectric loss (ε_I) as a function of frequency at different temperatures for plasticized polymer electrolyte (S2) and without plasticized (S6) are shown in Fig. 4 and inset, respectively. From the Fig. 4, it is observed that the dielectric loss becomes very large at lower frequencies due to free charge motion within the material. At very low frequencies, before there is a change in direction of field, there is particular time for the charges to build up at the interfaces and this contributes to the very large apparent values of ε_I. This phenomenon leads to conductivity relaxation [36]. The loss factor ε_I versus frequency consists of a dielectric relaxation at considerable higher frequency which is probably caused by the local movement of the side group dipoles (β–relaxation). The peaks get shifted to the higher frequency region as the temperature increases.

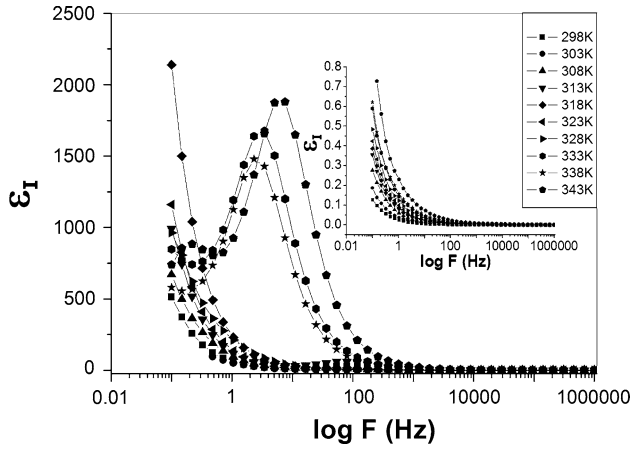

Fig. 4 Plots of dielectric loss versus frequency at different temperatures [*inset* without plasticizer (S6)]

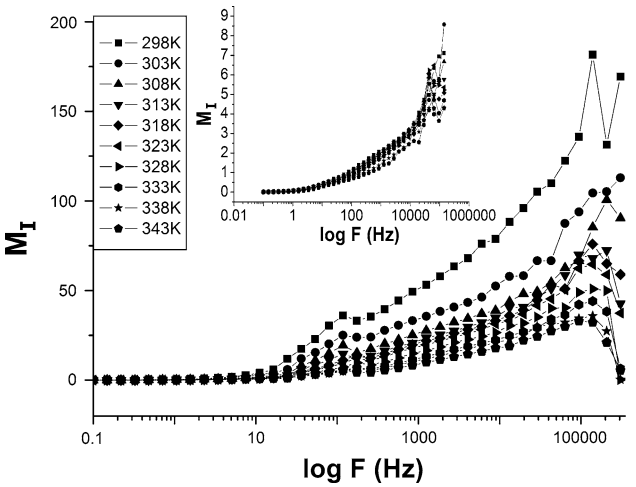

Fig. 6 Plots of imaginary part of electric modulus versus frequency at different temperatures [*inset* without plasticizer (S6)]

Hence, it implies that the temperature largely influences the dielectric loss of the samples.

The frequency dependence for the real, M_R and imaginary, M_I, parts of the electrical modulus with and without plasticizer (respective insets) at different temperatures are shown in Figs. 5 and 6, respectively. M_R in Fig. 5 reached a constant value at high frequencies, and at low frequencies, it approaches zero with a long tail feature. This indicates that the material is very capacitive in nature [37]. M_I curves show double peaks, thus indicating two independent processes in these blend polymer electrolyte film. The peaks in M_I imply ionic conduction since no relaxation peaks were found in the imaginary dielectric constant curves. The peaks are due to the electric conduction in films, since electrode polarization is negligible in the analysis of the electric modulus [38]. Thus, the peak at higher frequency in blend polymer electrolyte can be attributed to the electric conduction of H^+ wherein ions are spatially confined to their potential wells and can execute only localised motion and on the other hand, the peak at low frequency can be attributed to electric conduction due to Li^+ ions [39] wherein ions are capable of moving long distance, i.e. performing successful hopping from one site to the neighbouring site. The most probable mechanism for proton and Li ion conduction in the PSSA/starch blend polymer electrolyte has been represented in Fig. 7. Li ion conduction takes place majorly between hydroxyl groups of starch molecule [12]. The proton conductivity is Grotthus-type [40] in which a proton moves rapidly from H_3O^+ to a hydrogen bonded water molecule and is transferred further along a series of hydrogen-bonded water molecules by a rearrangement of hydrogen bonds.

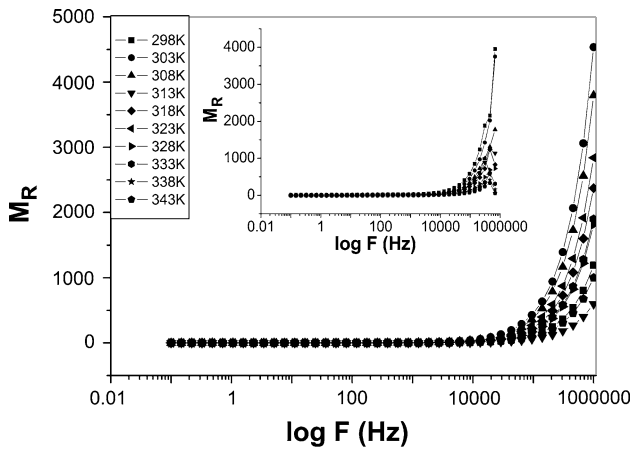

Fig. 5 Plots of real part of electric modulus versus frequency at different temperatures [*inset* without plasticizer (S6)]

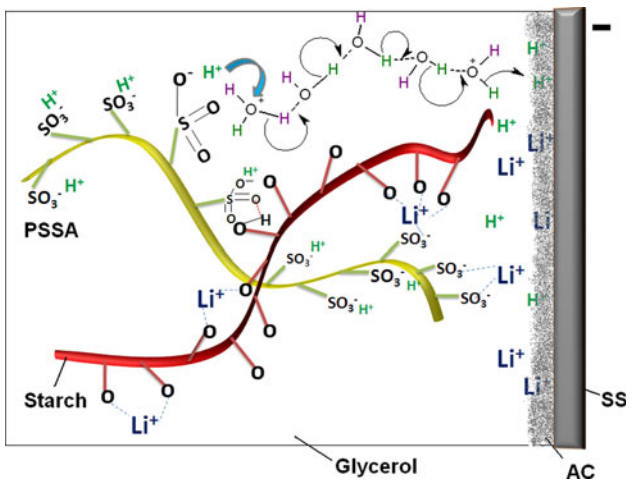

Fig. 7 Charge transport mechanism in blend polymer matrix of fabricated supercapacitor

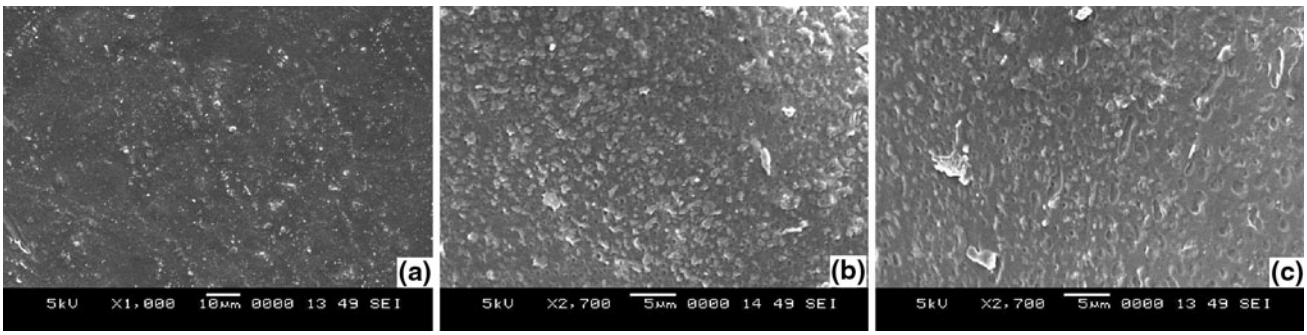

Fig. 8 SEM images of PSSA/starch blend polymer electrolytes **a** S2, **b** S4 and **c** S5

3.3 SEM analysis

Figure 8a, b and c shows SEM images of S2, S4 and S5 polymer electrolytes films, respectively. After adding starch, the interaction between PSSA and starch is quiet appreciable. The dual compatibility of starch towards both PSSA and the glycerol tends to lessen the driving force for separation of the PSSA phase and leads to better development of the film. The interaction produces a more relaxed network in the matrix Fig. 8a. However, the structure becomes increasingly heterogeneous (Fig. 8b, c) with an increase in starch content due to the aggregation of the ester group of starch forming new crystalline domains. These domains may cover some polar domains of PSSA and hence reduces the interaction between the electrolyte ions and polar section of the polymer matrix. The occurrence of phase-separation in the polymer electrolytes is indicative to pores in the micrographs. The several pores or craters, which have formed on the surface, are due to the rapid evaporation of the solvent (water). The difference in the pore size is related with the difference in the driving force for phase separation [41]. This may explain the reduction in ionic conductivity due to loss of water content and blending with starch requires an optimum concentration.

3.4 Thermal studies

DSC curves for S2, S6–S8 PSSA/starch blend films are present in Fig. 9. Based on the literature study, the T_gs of starch [42] and PSSA [43] are 146 and 152 °C, respectively. For $LiClO_4$-doped non-plasticized S7 (90/10) PSSA/starch blend ratio, the DSC curve shows increase in T_gs at 157 and 163 °C for starch and PSSA, respectively, indicating interaction of the dissociated salt with the polymers which are partially miscible. For S6, the T_gs of starch and PSSA decreased to 141 and 157 °C, respectively, indicating more interaction of salt with starch than PSSA. Further, T_g values of individual polymers decreased for S8 and moved away from each other. This indicates that salts are able to break the intramolecular interaction within the host polymer molecules and consequently increasing the segmental motion, thereby increasing the ionic conductivity. For plasticized $LiClO_4$-doped PSSA/starch blend film (S2), a broad peak is observed at 93 °C. This is attributed to plasticizing effect due to increase in free volume and reveals an increase in segmental mobility in the blend film [44].

3.5 Biodegradation studies

PSSA/starch–Li–salt complex films (S6–S8) and S2 showed considerable degradation in activated sludge method. After 15 days, the degradation was stopped and reported (Fig. 10). The degradation was found to be in the range of 11.1–18.5 % for S6–S8 samples. In this study, maximum biodegradation was in the case of S2 film with plasticizer content. As the constituents of the PSSA/starch–Li–salt complex films were hydroxyl groups, dissolutions of PSSA and an inorganic salt, hydrolysis could have been the major mode of degradation for starch. The hydrolysis products would be, organic acids, methanol, cellulose, etc., which are easily attacked by microorganisms to undergo

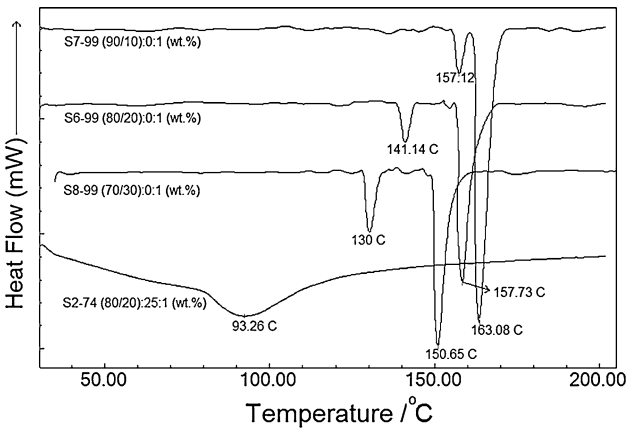

Fig. 9 DSC scan images of PSSA/starch polyelectrolyte films of different samples

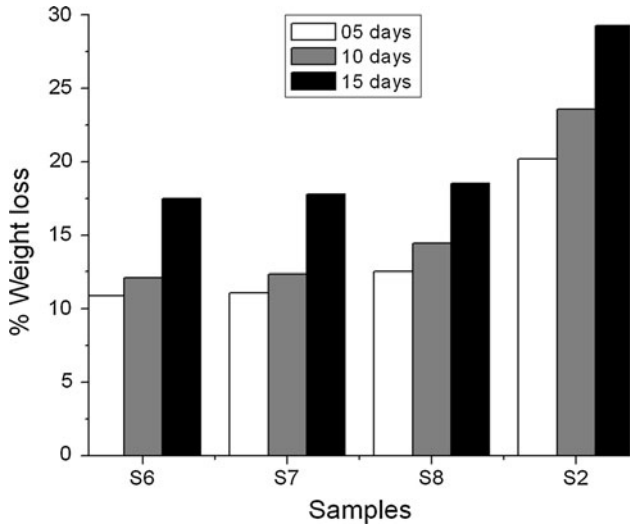

Fig. 10 Degradation of $LiClO_4$-doped PSSA/starch films in activated sludge

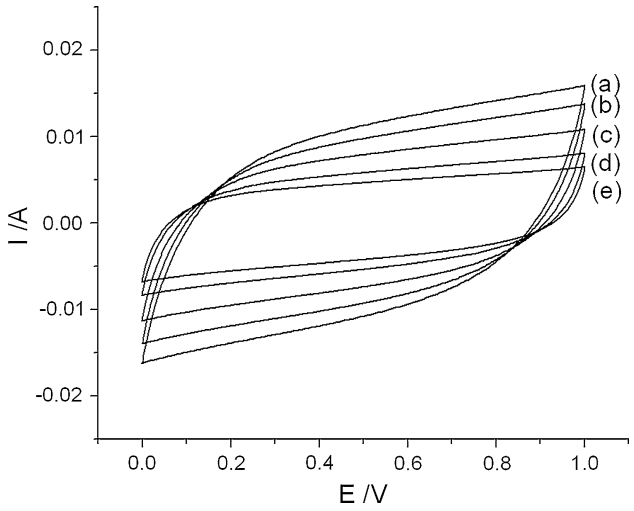

Fig. 11 CVs of the fabricated carbon–carbon symmetrical supercapacitor using $LiClO_4$-doped (S2) PSSA/starch blend electrolyte at scan rates. **a** 25 mV s^{-1}, **b** 20 mV s^{-1}, **c** 15 mV s^{-1} **d** 10 mV s^{-1}, and **e** 5 mV s^{-1}

further degradation. Samples S6 and S7 containing pure PSSA/starch polymer blend degradation were alike compared to S8 containing 70/30 blend ratio. This distinct difference clearly indicates the influence of Li salt complexation in promoting the biodegradation of polyelectrolyte material. This behaviour is also in conformity with that reported [26, 27] and agrees with thermal analysis since an increase in salt content reduced the interaction between polymer chains.

3.6 Supercapacitor studies

Sample S2 was used to construct supercapacitor cell due to its higher ionic conductivity. CV responses for the carbon–carbon symmetrical supercapacitor at various sweep rates are shown in Fig. 11. The specific capacitance values of the supercapacitor have been calculated using the equation;

$$C = \frac{2I}{\Delta V \times m} \quad (1)$$

where I is the corresponding average current resulting from the scan rate, ΔV is the voltage scan rate, m is the mass per electrode and C is the specific capacitance. A maximum specific capacitance of 115 Fg^{-1} at a scan rate of 10 mV s^{-1} was obtained, which implies a large amount of mobile protons and Li^+ are available in the film, which leads to a high capacitance of the device. The behaviours observed are characteristic of double layer capacitive features. A slight deviation from such a rectangular shape indicates low equivalent series resistance (ESR) in the device [45].

The AC impedance response (Nyquist plot) of the carbon–carbon supercapacitor is shown in Fig. 12. The plot shows a semicircle at high-frequency range and a straight line in the low-frequency region. Using this resistance at high-frequency, the value of C_{dl}, the double-layer capacitance, has been determined from the high-frequency region of the impedance spectrum using the equation

$$C = \frac{1}{2\pi f_{Max} R_{ct}} \quad (2)$$

where R_{ct} is charge transfer resistance and f_{max} is frequency at maximum imaginary axes value at semicircle region. The C_{dl} value obtained was 45 mF cm^{-2}. The capacitance value increases at low-frequencies because of a large number of ionic movements. The semicircle results from the parallel combination of resistance and capacitance and the linear region is because of Warburg impedance [1].

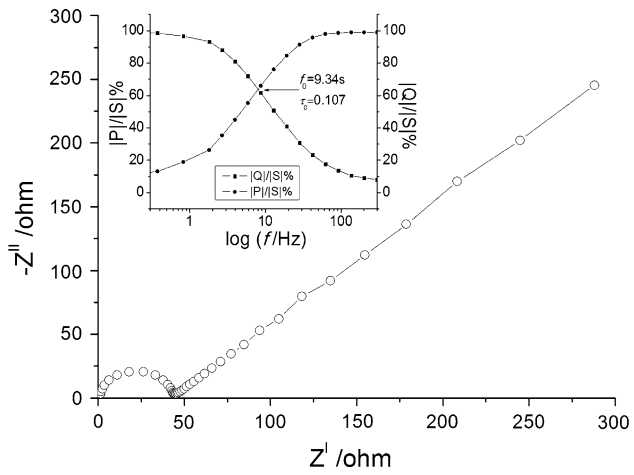

Fig. 12 AC impedance plot of supercapacitor [*inset* Plots of normalized reactive power |*Q*|/|*S*| % and active power |*P*|/|*S*| % vs. frequency (Hz) of supercapacitor]

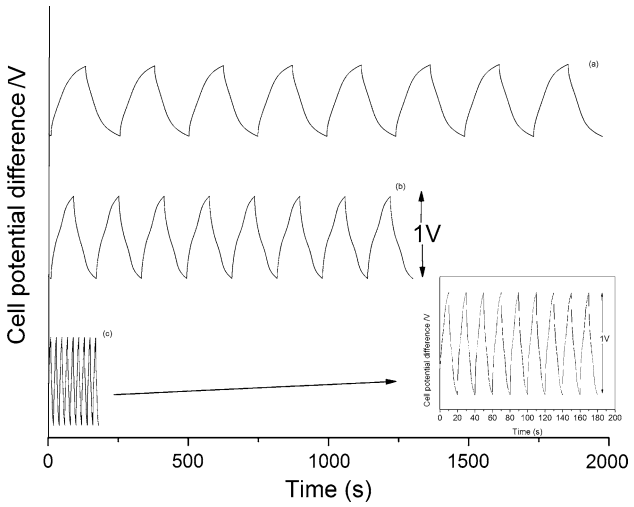

Fig. 13 Galvanostatic charge–discharge plots for the supercapactior at **a** 1 mA cm^{-2}, **b** 1.5 mA cm^{-2} and **c** 3 mA cm^{-2}

Using normalized reactive power $|Q|/|S|$ % and active power $|P|/|S|$ % versus frequency plot for the 1 cm^2 cell, the time constant of the fabricated supercapacitor has been calculated and is shown in Fig. 12 inset. The theoretical details of this plotting technique have been taken from the literatures [24, 46]. The calculated time constant was found to be equal to 0.107 s. The time constant (τ_0) represents a transition for the supercapacitor between a resistive behaviour for frequency higher than $1/\tau_0$ and a capacitive behaviour for frequencies lower than $1/\tau_0$. Hence, the observed time constant value of 0.107 s indicates that the present system can be efficiently used at low frequencies.

3.6.1 Galvanostatic charge–discharge studies

Figure 13 shows galvanostatic charge–discharge tests between cell voltages of 0–1 V at 1, 1.5, and 3 mA cm^{-2}. The supercapacitor specific capacitance (C) specific power (SP), and specific energy (SE) [47] were evaluated from charge–discharge curves according to the following formulas

$$C = \frac{I \times \Delta t}{\Delta V \times m} \quad (3)$$

$$SP\ (Wg^{-1}) = [I \times \Delta V]/m \quad (4)$$

$$SE\ (Wh\,g^{-1}) = [I \times t \times \Delta V]/m \quad (5)$$

where I (A), ΔV (V), Δt (s), m (g), respectively are discharge-current, discharge-voltage, discharge-time and mass of active material, results are presented in Table 1. The charge–discharge curves are nearly linear symmetry except for a little bump in the terminal of discharge line, which is due to no redox reaction happening in the potential window of 0–1 V [17]. The specific capacitance for the supercapacitor with blend polymer electrolyte at scan rates of 1.0, 1.5 and 3 mA cm^{-2} were found to be 106, 98 and 95 Fg^{-1}, respectively. The decrease in specific capacitance of the supercapacitor is due to quicker ions diffusion rate as current density increases and more adequately due to the presence of activated carbon which enhances the electrode/electrolyte interfacial contact. The coulombic efficiency of the supercapacitor calculated from charge–discharge cycles is also high in the range of 95–97 %. In order to evaluate the cycling stability of the PSSA/starch blend polymer electrolyte in supercapacitor, galvanostatic charge–discharge studies were performed and the long cycle performance is shown in Fig. 14. The data reflect that the device exhibited almost constant capacitance during the test. However, at higher cycle numbers, the capacitance is likely to decrease slightly because of the decrease of double layer activity of the supercapacitor.

4 Conclusions

In summary, we have reported a supercapacitor based on activated carbon electrode and $LiClO_4$-doped poly(styrene sulphonic acid)/starch blend polymer electrolyte. Glycerol as plasticizer helped to improve the film forming ability of the polymers and also ionic conductivity. The maximum

Table 1 Supercapacitor parameters

Current density (mA cm^{-1})	Cycle no.	SC (Fg^{-1})	SP (Wg^{-1})	SE (Wh g^{-1})	Columbic efficincy N%	ESR (Ω)	Voltage drop (V)
1.0	1	106	0.95	9.5	97	09	0.03
	1,000	103	0.92	9.2	95	10	0.04
	3,000	103	0.92	9.2	95	10	0.04
1.5	1	98	0.96	9.3	98	08	0.02
	1,000	96	0.95	9.0	96	10	0.03
	3,000	96	0.95	9.0	96	10	0.03
3	1	95	0.98	9.1	98	07	0.02
	1,000	93	0.97	8.9	96	10	0.03
	3,000	93	0.97	8.9	96	10	0.03

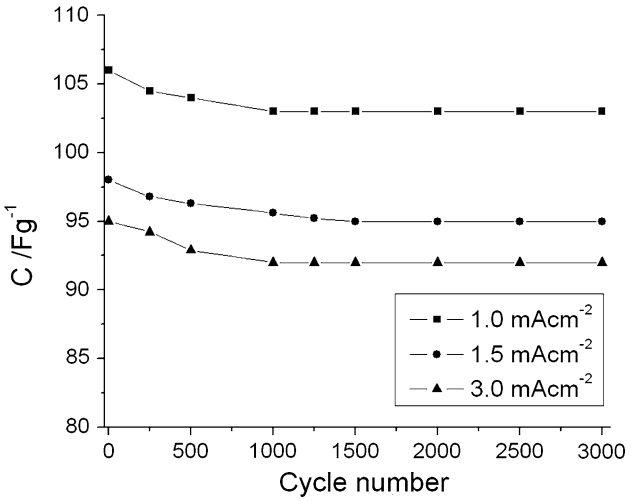

Fig. 14 The specific capacitance (*C*) of the supercapacitor with S2 electrolyte during long-term cycling

conductivity has been found to be 5.7×10^{-3} Scm^{-1} at 298 K for 80 % PSSA (S2) content in PSSA/starch blend ratio. The dielectric studies indicated the high capacitive nature and the presence of relaxation process in the material indicating proton and Li ion motion in the blend polymer matrix. A fabricated carbon–carbon supercapacitor showed a fairly good specific capacitance of 115 Fg^{-1}. The supercapacitor was quite stable during charge–discharge cycles and exhibited high coulombic efficiency.

Acknowledgments Authors acknowledge with thanks the financial support received from the Defence and Research Development Organisation, Govt. of India, New Delhi.

References

1. Conway B (1999) Electrochemical supercapacitors. Kluwer Academic/Plenum, New York
2. Winter M, Brodd RJ (2004) Chem Rev 104:4245
3. Rudge A, Raistrick I, Gottesfeld S (1994) Electrochim Acta 39:273
4. Hashmi SA (2004) Natl Acad Sci Lett 27:27
5. Stephan AM (2006) Eur Polym J 42:21
6. Tambelli CE, Donoso JP, Regiani AM, Pawlicka A, Gandini A, LeNest JF (2001) Electrochim Acta 46:1665
7. Victoria KL (2005) Appl Microbiol Biotechnol 67:735
8. Peng SW, Wang XY, Dong LS (2005) Polym Compos 26:37
9. Ge XC, Li XH, Zhu Q (2004) Polym Eng Sci 44:2134
10. Kim SH, Kim YH (2000) Polym Eng Sci 40:2539
11. Khiar ASA, Arof AK (2010) Ionics 16:123
12. Arrieta AA, Gañán PF, Márquez SE, Zuluaga R (2011) J Braz Chem Soc 22:1170
13. Gray FM (1997) Polymer electrolytes. The Royal Society of Chemistry, Cambridge
14. Rikukawa M, Sanui K (2000) Prog Polym Sci 25:1463
15. Sun J, Jordan LR, Forsyth M, MacFarlane DR (2001) Electrochim Acta 46:1703
16. Acar O, Sen U, Bozkurt A, Ata A (2009) Int J Hydrog Energy 34:2724
17. Wee G, Larsson O, Madhavi S, Magnus B, Xavier C, Subodh M (2010) Adv Funct Mater 20:4344
18. Sousa AMM, Sereno AM, Hilliou L, Goncalves MP (2010) Mater Sci Forum 636:739
19. Yahya MZA, Arof AK (2004) Carbohydr Polym 55:95
20. Vieira F, Avellaneda CO, Pawlicka A (2007) Electrochim Acta 53:1404
21. Bhat DK, Selvakumar M (2006) J Polym Environ 14:385
22. Selvakumar M, Bhat DK (2008) J Appl Polym Sci 110:594
23. Selvakumar M, Bhat DK (2009) J Appl Polym Sci 114:2445
24. Sudhakar YN, Selvakumar M, Bhat DK (2012) Ionics. doi: 10.1007/s11581-012-0745-5
25. Wine T, Arof AK (2004) Ionics 10:193
26. Okada M, Yamada M, Yokoe M, Aoi K (2001) J Appl Polym Sci 81:2721
27. Chandra R, Rustgi R (1997) Polym Degrad Stab 56:185
28. Sudhakar YN, Selvakumar M (2012) Electrochim Acta 78:398
29. Aarti SB, Bhat DK, Santosh MS (2011) J Electroanal Chem 657:135
30. Chowdhury NA, Shukla AK, Sampath S, Pitchumani S (2006) J Electrochem Soc 153:A614
31. Uma T, Mahalingam T, Stimming U (2005) Mater Chem Phys 90:245
32. Andrade JR, Raphael E, Pawlicka A (2009) Electrochim Acta 54:6479
33. Meenakshi P, Noorjahan SE, Rajini R, Venkateswarlu U, Rose C, Sastry TP (2002) Bull Mater Sci 25:25
34. Mishra R, Rao KJ (1998) Solid State Ion 106:113
35. Patro LN, Hariharan K (2009) Mater Sci Eng B 162:173
36. Bozkurt A (2002) J Phys Chem Solids 63:685
37. Watanabe M (1992) Solid state ionics. In: Chowdari BVR, Chandra S, Singh S, Srivastava PC (eds) Materials and applications. World Scientific, Singapore, p 373
38. Macedo PB, Moynihan CT, Bose R (1972) Phys Chem Glasses 13:171
39. Khiar ASA, Puteh R, Arof AK (2006) Phys B 373:23
40. Selvakumar M, Bhat DK (2009) Phys B 404:1143
41. Rhoo HJ, Kim HT, Park JK, Hwang TS (1997) Electrochim Acta 42:15
42. Osman Z, Ibrahim ZA, Arof AK (2001) Carbohydr Polym 44:167
43. http://www.polymersource.com/dataSheet/P4998-USSO3H.pdf. Accessed 26 July 2012
44. Sakurai K, Maegawa T, Takahashi T (2000) Polymer 41:7051
45. Guo Q, Zhou X, Li X, Chen S, Seema A, Greiner A, Hou H (2009) J Mater Chem 19:2810
46. Taberna PL, Simon P, Fauvarque JF (2003) J Electrochem Soc 150:A292
47. Yu H, Wu J, Fan L, Lin Y, Xu K, Tang Z, Cheng C, Tang S, Lin J, Huang M, Lan Z (2012) J Power Sources 198:402